Aerosol Science and Technology
Publication details, including instructions for authors and subscription information:
http://www.tandfonline.com/loi/uast20

Fluidized Bed Generation of Stable Silica Nanoparticle Aerosols

Alberto Clemente [a] , Francisco Balas [b] , M. Pilar Lobera [a] , Silvia Irusta [a] & Jesús Santamaría [a c]

[a] Instituto de Nanociencia de Aragón (INA), c/ Mariano Esquillor s/n, 50018, Zaragoza, (Spain)

[b] Instituto de Carboquímica—Consejo Superior de Investigaciones Científicas (ICB-CSIC), c/ Miguel Luesma 4, 50018, Zaragoza, (Spain)

[c] Networking Research Centre for Bioengineering, Biomaterials and Nanomedicine (CIBER-BBN), c/ Mariano Esquillor s/n, 50018, Zaragoza, (Spain)

Accepted author version posted online: 23 Apr 2013.

To cite this article: Alberto Clemente , Francisco Balas , M. Pilar Lobera , Silvia Irusta & Jesús Santamaría (2013): Fluidized Bed Generation of Stable Silica Nanoparticle Aerosols, Aerosol Science and Technology, DOI:10.1080/02786826.2013.797952

To link to this article: http://dx.doi.org/10.1080/02786826.2013.797952

Fluidized Bed Generation of Stable Silica Nanoparticle Aerosols

Alberto Clemente[1], Francisco Balas[2], M. Pilar Lobera[1], Silvia Irusta[1] and Jesús Santamaría[1,3]

[1]*Instituto de Nanociencia de Aragón (INA), c/ Mariano Esquillor s/n, 50018 Zaragoza (Spain)*

[2]*Instituto de Carboquímica – Consejo Superior de Investigaciones Científicas (ICB-CSIC), c/ Miguel Luesma 4, 50018 Zaragoza (Spain)*

[3]*Networking Research Centre for Bioengineering, Biomaterials and Nanomedicine (CIBER-BBN), c/ Mariano Esquillor s/n, 50018 Zaragoza (Spain)*

Address correspondence to Francisco Balas, Instituto de Carboquímica – Consejo Superior de Investigaciones Científicas (ICB-CSIC), c/ Miguel Luesma 4, Zaragoza 50018, Spain. E-mail: fbalas@unizar.es; or to Jesús Santamaría, Chemical Engineering Department and Aragon Institute of Nanoscience, University of Zaragoza, C/ Pedro Cerbuna 12, Zaragoza 50009, Spain. E-mail: Jesus.Santamaria@unizar.es

Abstract

A long-lasting generator of continuous silica nanoparticle aerosols based in a fluidized bed of glass beads coated with nanosized silica has been developed. The attrition resulting from the bubbling fluidized bed regime progressively detaches the silica coating from the glass beads, giving rise to a steady production of silica nanosized aerosols with median diameters from 100 to

250 nm depending of the initial size of the coating nanoparticles. Continuous aerosol production could be maintained for more than 12 h, and the nanoparticle concentration can be easily tuned in the range from 2,000 to 14,000 #/cm^3 by adjusting the fluidization and/or dilution flow rates.

1. Introduction

The generation of long lasting nanoparticle aerosols with stable particle number concentration is a key requirement for many applications. For instance, the development of high-efficiency filtering systems for airborne nanoparticles and the tuning of aerosol spectrometers need constant and monodisperse aerosols to assess nanoparticle penetration under different conditions (Denny et al. 2010, Savolainen et al. 2010). Other applications include the validation of models of nanoparticle behavior in the atmosphere, where the production of well characterized aerosols is essential to study particle aggregation and agglomeration (Cho et al. 2011; Wang et al. 2011). Nanoparticle aerosol generators are also widely used in investigations of the effect of NP aerosols on human health (Grassian et al. 2007), their biological and environmental impacts (Schmoll et al. 2009; Chen et al. 2010; Kreyling et al. 2011), and the role of particles as vectors for the transport of airborne pathogens (Liu et al 2012).

Standard aerosol generators often use wet processes involving atomizing solutions of a given composition to form droplets that give rise to solid nanoparticles when the solvent is evaporated, or of suspensions already containing the nanoparticles at the desired concentrations (Liu 1975; Kruis et al. 1998). Often, drop formation and evaporation is facilitated by means of ultrasound, vibrating orifice systems, pneumatic or electro hydrodynamic atomization, spray

pyrolysis and condensation devices (John 1993; Biskos et al. 2008). While wet generation methods have the advantage of a high flexibility regarding the nature of the particles that can be produced, they also present important problems, including the presence of impurities in the solvent, the production of aerosols with a low nanoparticle concentration and the difficulties in achieving a sufficiently low droplet size (Biskos et al. 2008), in addition to the obvious problem of having to evaporate a large amount of solvent which is then entrained in the produced aerosol. This has prompted numerous studies aimed to achieve stable aerosol generation by dry processes. Spark generation and electrospray can be used to produce highly stable aerosols containing engineered nanomaterials, including carbon nanotubes and nanosized metal oxides (Biskos et al. 2008; Bau et al. 2010; Jennerjohn et al. 2010; MacMillan et al. 2012). These systems produce stable nanoparticle aerosols with controllable sizes up to several hours of operation.

Fluidized beds are widely used in the chemical industry in a variety of reactive and non-reactive processes. Aerosol generation is a less common application but nevertheless fluidized beds have also been used for decades to generate aerosols of relatively coarse particles (Guichard 1976), and more recently for nanoparticles (Wang et al. 1998; Yao et al. 2002). Myojo et al. (2009) reported the use of a fluidized bed to homogenize the supply of multi-walled carbon nanotubes from a rotating brush aerosol generator, giving concentrated carbon nanotube aerosols for limited experimental times (under one hour of operation). Lind et al. (2010) reported on the use of a glass-bead fluidized bed for producing silica ultrafine particles (1 and 2.6 μm). However, this produced a decreasing particle concentration, unless the operating flow rate was continuously adjusted to compensate for the diminishing particle supply. Denny et al. (2010)

designed a TiO_2 nanoparticle aerosol generator by continuously feeding TiO_2 particles to a fluidized bed composed of 300 μm bronze beads. The device was able to generate a flow of TiO_2 nanoparticles that was used to coat a photo catalytic filter. Indeed, the continuous addition of bed material leads to longer periods of stable aerosol generation and it was originally proposed by Prenni et al. (2000) for generating sub-micrometer soot aerosols from a bronze-bead fluidized bed. It should be realized that fluidizing nanomaterials is a challenging task, as shown in a recent review (Van Ommen et al. 2012), and this is the reason why most of the fluidized bed aerosol generators use a second, coarse solid as a co-adjuvant. Nanoparticles from fluidized beds devices form agglomerates with a particle size distribution that depends on the material properties, primary particle size, characteristics of the generator device and operating conditions (Van Ommen et al. 2012).

It seems evident that a fluidized bed generator capable to deliver a stable flow of nanoparticles without the need to supply additional solid feed would be extremely interesting for a number of nanotechnology applications. This can only be achieved by (i) loading a sufficiently high amount of nanomaterials in the fluidized bed, and (ii) implementing a mechanism that allows a progressive release of these nanomaterials, in such a way that a stable aerosol results. In this work we have achieved this by coating glass beads of a suitable size for fluidization (80-150 μm) with a layer of silica NPs, and loading the coated beads in a fluidized bed aerosol generator (FBAG). The bubbling fluidization regime produces attrition of the nanoparticle coating, leading to a steady release of NPs into the gas phase. As a consequence, the FBAG produces a concentration-tunable aerosol of nanoparticles with a size of 100-300 nm. This is a range usually

employed in health-related studies, as well as in nanoparticle penetration tests, since it is considered as the most penetrating particle size range (Wang, 2005).

In the present work, a FBAG that allows the production of nanoparticle aerosols for up to 12 h of continuous operation, without the need for continuous feeding of nanoparticles is developed. The FBAG is tested with two types of particles, namely 15-nm SiO_2 nanoparticles and 100-nm nanoparticles prepared by the Stöber method. The particle size distributions of the resulting aerosols are centered on 200 and 100 nm, respectively.

2. Materials and Methods

2.1. Bed Preparation

Glass beads with a bulk density of 2.5 g/cm^3 are provided by Abrasivos y Maquinaria, SA (Barcelona, Spain) with nominal composition of SiO_2 70-73%, Na_2O 13-15%, CaO 7-11%, MgO 3-5%, Al_2O_3 0.5-2% and K_2O 0.2-0.6% and with a hardness of 6 in the Mohs scale. As-received beads are subjected to two cycles of washing with ethanol (Sigma-Aldrich) followed by drying at 25ºC for 8 h. The dry glass beads are sieved to a size between 80 and 150 µm using stainless steel sieves. A mass of 66 g of the sieved glass beads were then immersed in a colloidal suspension of 0.225 g of dense 5-15 nm silica nanoparticles (Sigma-Aldrich) in 25 mL of 96% ethanol. Alternatively, Stöber silica nanoparticles (NPs) are prepared using tetraethyl orthosilicate (TEOS, Sigma-Aldrich 98%), ammonium hydroxide (NH_4OH, Sigma-Aldrich) and Milli-Q water using the synthesis procedure that was published elsewhere (Gutierrez et al. 2011). Suspensions are stirred at 25 ºC for solvent evaporation. The mass of deposited silica NPs is

estimated as 0.34 wt % of the total mass of the glass beads. The overall process for the bed preparation is schematically plotted in Figure 1a.

2.2. Design and Operation

A scheme of the system used is presented in Figure 1b. The fluidized bed aerosol generator is built in a 30-mm-i.d., 200-mm-long polypropylene tube equipped with a 50-µm stainless steel grid. Two independent dry and HEPA-filtered (Whatman HEPA-Cap 150) air supplies are used to supply fluidizing air to the FBAG and to incorporate additional carrier flow to dilute the concentration of the generated aerosol as needed. All airflows are mass flow controlled (Bronkhorst), and the generated particulate aerosol is driven using stainless steel pipes first into a large-particle collector (LPC) chamber that eliminates aerosol particles over 5 µm in size and then into the aerosol particle counters (see below) located downstream. This LPC is an inertia-driven device that directs the aerosol through a 10-mm glass pipe into the bottom of a 350-cm^3-glass chamber with 56 mm internal diameter. Inside the LPC, larger particles impact the bottom wall where they are deposited while the aerosol, now with a lower velocity, is able to entrain the smaller particles that constitute the aerosol. The excess aerosol is driven out of the system through a HEPA-filter unit located in a three-way valve to avoid overpressure in the line that could damage the detection units. The range of operating conditions was as follows: feed flow rate, 1-2.5 L/min; diluting air flow rate, 0.5-8.5 L/min; the silica-coated glass-beads, 80-150 µm had a minimum fluidization velocity (u_{mf}) of 0.58 cm/s, as determined in separate experiments with dry and HEPA-filtered air at 25 ºC, the relative gas velocity ($u_r = u/u_{mf}$) was 1.8 to 4.5 cm/s; height of the bed (H_B) in the absence of fluidization gas 5 cm; temperature 25 ºC. Before each experiment, the fluidized bed system was purged with HEPA filtered air in order to eliminate the

ambient particle aerosol out of the pipes and other conductions of the sampling system and to remove loose material in the fluidized bed.

To determine the fraction of aerosol particles with sizes between 300 nm and 20 μm an 8-channel optical particle counter (OPC, Model #1.108; Grimm Aerosol Technik) is used. The fraction of smaller aerosol particles is determined using a stepping mobility particle spectrometer (SMPS+C, Model #5.403; Grimm Aerosol Technik) that comprises a differential mobility analyzer (DMA, Model 33-900; Grimm Aerosol Technik) and a condensation particle counter (CPC). This SMPS+C system allows the measurement of unit density spherical particles from 10 to 1110 nm with a normal scan time of 7 min. The inlet aerosol in the SMPS system is electrically neutralized using a ^{241}Am alpha-emission source to provide an equalized distribution of charges on the surface of nanoparticles. The ambient aerosol in the laboratory conditions is usually composed of 5 to 50-nm particles at concentrations between 3,000 and 5,000 #/cm^3, as measured by the SMPS+C apparatus. A dry and HEPA-filtered airflow of 2 L/min is used to purge the whole system before operation, and within five minutes after purging, values below 5 #/cm^3 are measured by the condensation particle counter unit (CPC) of the SMPS+C system, confirming the successful purge of the system.

2.3. Material Characterization

The morphology of glass beads and the particles collected in the aerosol phase are observed using SEM with a FEI Inspect Field Emission Gun microscope. Silica nanoparticles were characterized using TEM in a FEI Tecnai T20 microscope using copper grids as sample holder. The effective sizes of the SiO_2 nanoparticle suspensions used for the coating are

measured in liquid suspensions using dynamic light scattering (DLS) in a Brookhaven 90Plus analyzer (Brookhaven Instruments Co., New York). The data (not shown) indicated that the mean effective particle size in the suspensions used to coat the glass beads is centered on 230 and 120 nm for 5-15 nm silica and Stöber nanoparticles, respectively.

3. Results and Discussion

3.1. Glass bead and nanoparticle characterization

The morphology of the primary silica nanoparticles used to coat the glass beads used in the FBAG is displayed in the TEM images of Figure 2 together with their size histograms. Images show isolated particles with a mean particle size of 6.7 nm and a standard deviation of 2.7 nm. An overall view of uncoated and silica-coated glass beads is given in the SEM images of Figure 3. The naked beads present a clean, particle-free surface (Figure 3a) and the cross-section of the beads (Figure 3b) shows the smooth surface of the glass particles. After coating with 5-15-nm silica nanoparticles (Figure 3c), most of the surface appears coated with a relatively homogeneous layer of nanoparticle agglomerates of a small size, although some larger agglomerates are also visible. The close-up cross-sectional view of figure 3d reveals that most of the nanoparticle coating presents a thickness of 100-400 nm, which is or the order expected taking into account the weight load of the silica (see Supplemental Information). Coating with 100-nm Stöber nanoparticles produces a layer of silica nanoparticles on the surface of glass beads, as it can be seen in Figure 3e and 3f. This coating with a thickness of a few hundred nm is formed by nanoparticles about 100 nm in size.

3.2. Generation of NP aerosols

Stable and monodisperse nanoparticle aerosols are generated using the FBAG with silica-coated glass beads. The collisions among glass beads in the bubbling fluidization regime of the FBAG lead to the progressive release of the nanoparticle agglomerates attached to their surface, giving rise to a continuous aerosol, as will be shown later. In order to demonstrate that the aerosol is produced from the coatings on the glass beads and not from the beads themselves a blank experiment was performed in which a bed of uncoated glass beads was fluidized in the FBAG. In the Figure S1 of the Supplemental Information file it can be observed that the measured number concentration of the aerosol generated using a non-coated bed reaches a maximum immediately after the start of fluidization due to the presence of unbound material and then rapidly decreases below 5 #/cm^3 after a few minutes of operation. Consequently, debris from the glass beads will only have limited contribution to the aerosol produced by the fluid bed generator.

All of the experiments in this work are conducted in a semi-continuous mode: a batch of nanoparticle-coated glass beads is loaded on to the FBAG and the system is operated without additional feed of nanoparticles to the bed. In spite of this, a stable aerosol is generated for up to 12 h of operation, as shown in Figure 4, where the time evolution of the aerosol is followed by measuring the number concentration of particles with particle sizes between 5 and 1110 nm using the SMPS+C device in the counting mode. For this purpose, the generated dry aerosols are driven through the CPC without previous electrostatic classification. The data in this figure correspond to the particle counts obtained with two different batches of 5-15 nm silica-coated beds, prepared independently. It can be seen that in both cases there is an initial transient period of a few minutes during which the particle counts rapidly decrease to a nearly stable level that is

maintained, with small variations for the duration of the experiment (12 h in this case). In addition there is an excellent reproducibility of the aerosol counts (values of 9,584 ± 343 #/cm^3 for Bed-A and 9,857 ± 318 #/cm^3 for Bed-B were obtained after fluidization for 10 h in both experiments). Similar results (not shown) are obtained for Stöber silica coated glass beads, which indicate a good repeatability of the coating protocol together with a high stability of the generated aerosols.

From the data of Figure 4, the generation of nanoparticle aerosols using the FBAG can be described as a three-stage process:

(i) In the first stage fluidization starts, and the initial collisions among the nanoparticle coated glass spheres rapidly remove the weakly bound material, resulting in a burst release of particles, leading to concentrations up to 30,000 #/cm^3 for the first seconds of operation.

(ii) A stabilization stage follows, during which the initial burst decreased abruptly for the next 15 to 60 min until stable levels are reached. This stabilization period might be related to the removal of large agglomerates on the surface of the beads, which are likely to be more affected by particle collisions. This effect has been also reported in the dustiness tests performed with nanoparticles (Jensen et al. 2009; Tsai et al 2012).

(iii) The third stage corresponds to the generation of a stabilized nanoparticle aerosol. Once the weakly bond material and the large agglomerates in the surface of the beads have been eliminated, the remaining nanoparticle coating on the beads presents similar characteristics and stable generation is achieved by attrition in the bubbling fluidized bed regime.

As shown in Figure 4(b), the number concentration of aerosols produced upon fluidization of 5-15 nm silica coated glass beads is stabilized about 10,000 #/cm^3. Similar results are obtained when fluidizing glass beads coated with 100-nm Stöber nanoparticles. As can be seen in Figure 5, the aerosol number concentration is stabilized at values close to 10,000 #/cm^3 for periods up to 12 h of continuous operation. In both cases, these numbers are well above those of previously reported aerosols generators based on fluidized bed technology (Prenni et al. 2000, Lind et al. 2010, Denny et al. 2010, Myojo et al. 2009). By using a continuous feeding system generation of highly concentrated aerosols can be achieved over a period of several hours but the average particle size is usually larger than 1 μm (Vincent 2007), a value too large for studies of nanoparticle aerosols.

The count particle size distributions are fitted using a lognormal probability density function (Vincent 2007). The values of count median diameter (CMD) for aerosols obtained from beds A and B are 201.9 and 202.1 nm respectively, whereas geometric standard deviation (GSD) for the same count distributions are 1.31 and 1.32 respectively. The statistical testing of the resulting aerosols gives that both CMD and GSD are similar with $p > 0{,}005$. For lognormal distributed aerosols, the polydispersity index (W) of the obtained size distributions is estimated after the values of GSD as $W = \sqrt{\exp(\ln^2 GSD) - 1}$ (Pratsinis 1988). In these conditions, the values for W are about 0.28 in both cases. Although W is a quantitative measure of the spread of the size distributions, the threshold values for mono and polydisperse aerosols are arbitrarily selected depending on the end use of the aerosol (Pratsinis et al. 1986). In general, aerosols are usually accepted to be truly monodisperse aerosols if $W < 0.3$. In terms of GSD, monodispersity is conventionally considered for values between 1 and 1.4 (Hinds 1999; Rosati et al. 2003).

The time evolution of the particle size distribution in the aerosol is investigated in successive SMPS+C scans at the FBAG outlet. The fluidization of 5-15 nm silica nanoparticle coated glass beads gives highly stable size distributions with a CMD of 210 nm and GSD of 1.4 nm, with values of W under 0.3 throughout the sampled period (Figure 6). In the case of Stöber nanoparticle aerosols, the time stability is tested for periods as long as 10 h of continuous operation as it is shown in Figure 7a. The size distributions for the aerosols formed with those nanoparticles give a CMD of 112 nm and GSD of 1.25, with W under 0.3 during the tests, indicating a highly monodisperse aerosol. Moreover, it is interesting to mention that aerosol particles have median size very close to that observed in the SEM images (Figure 3e), which indicates that aerosol is mainly composed of non-agglomerated particles.

As an additional check of the particle size distribution for the larger fraction of particle sizes, the number of aerosol particles with sizes over 300 nm was also measured using the OPC in the above-described experiment. The overall size distribution of generated aerosol with data from the OPC and the SMPS+C for the aerosols generated upon fluidization of both 5-15-nm silica-coated and 100-nm Stöber silica coated beads are respectively plotted in Figures 6b and 7b. In the area where the measurements from both instruments overlap (300-1000 nm) the CPC gives consistently higher counts (around 2500-3000 #/cm^3), but the discrepancy can be considered acceptable because both instruments are based on different physical principles.

The design of the FBAG allows an effective tuning of the particle concentration in the generated aerosol by changing the fluidization or the diluting airflow. Figure 8a shows the effect of the fluidization gas flow rate upon the concentration of the aerosol particles generated for a constant dilution flow rate using the 5-15 nm silica coated glass beads. As the fluidization flow

rate increases, the bed expands and the bubbling becomes more vigorous, increasing the particle number concentration at the FBAG exit. Also, for a given fluidization flow rate, increasing the diluting airflow allows to tune down the concentration of nanoparticles in the generated aerosols, as can be seen in Figure 8b. The particle number concentration continuously decreased with increasing dilution rates down to 1,400 #/cm^3, for a diluting airflow of 8.5 L/min. Similar results (not shown) are also found for the 100-nm Stöber silica coated glass beads.

The particle morphology was examined offline on aerosol samples collected at the exit of the FBAG using two different devices that were placed perpendicularly to the airflow. Figure 9 displays images of the particles sampled using a holey carbon-coated copper TEM grid at 300 mL/min for 15 s (Figure 9c and 9d). Alternatively, a polycarbonate filter with a cut-off size of 50 nm was placed in a Whatman filter holder unit and the aerosol was sampled at 300 mL/min for 5 min, then the filter was examined using SEM (Figure 9a and 9b). The fluidization of 15-nm silica-coated glass beads produces agglomerates with a mean size of about 350 nm (Figures 9a and 9c). On the other hand, single nanoparticles of about 100 nm are obtained upon fluidization of 100-nm Stöber silica coated glass beads (Figures 9b and 9d). It is worth mentioning that offline collection procedures give similar size distributions for the aerosol agglomerates, which are slightly higher than the data obtained using the SMPS+C and OPC, probably due to additional agglomeration on the collection device. In any case, the size and morphology of the particles within the aerosol was completely different from the original the 5-15 nm particles loaded onto the glass beads. Instead, most of the particles collected are in the 100-400 nm intervals, which is coincident with the thickness of the coating on beads. This suggests that the aerosol particles may originate from detachment of whole nanoparticle lumps on the surface. For

Stöber silica nanoparticles, the size of initially attached nanoparticles roughly coincides with the sizes detected using SMPS+C and offline techniques, where mainly non-agglomerated nanoparticles can be observed. This strongly suggests that the formation of airborne silica nanoparticles during fluidization of Stöber-coated beads can be attributed to the detachment of individual nanoparticles from the glass surface. Although additional aggregation could be expected from the gas phase agglomeration of the nanoparticles released, as Lushnikov (2010), Eggersdorfer and Pratsinis (2012) and Van Ommen et al. (2012) reported, this is unnoticed at least for 100-nm Stöber silica coated glass beads.

The nanoparticle-detaching process leading to aerosol generation has been analyzed using SEM images of the glass beads after fluidization a certain period. The surface of as-coated glass beads with both 5-15 nm silica and 100-nm Stöber silica nanoparticles show rather different features, as it can be seen in Figure S2 of the Supplemental Information file. Agglomerated particles are observed for the small-sized silica while the originally larger Stöber nanoparticles are extended all over the surface and largely maintain their individuality. The fluidization provokes the detachment of nanoparticles with the sizes that are in the region of the clusters present on the glass surfaces. The surface coverage of glass beads is eventually reduced after fluidization, although is worth mentioning that the aerosol number concentration is only reduced by a 20% during the 100-h fluidization tests (results not shown). In addition, the sizes of the particles forming the aerosol are approximately constant during the period of operation, indicating that the size of the detached objects remains roughly constant.

4. Conclusions and Outlook

Stable silica aerosols are produced after fluidization of a bed composed of glass beads with a thick coat of agglomerated silica nanoparticles. The process of nanoparticle loading on the glass beads produces highly stable coatings, which are progressively detached during prolonged fluidization due to mechanical attrition. The bubbling fluidization of these composite beads allows the generation of stable nanoparticle aerosols for periods of more than 12 h of continuous operation, with aerosol particle size distributions centered between 100 and 200 nm, depending on the size of the original coating particles and without the need for continuous feeding of additional nanoparticles. The high stability of the aerosols generated, with the nanoparticle diameters in the most penetrating particle size range makes the FBAG useful for a variety of studies ranging from the toxicological and occupational impact of dry nanoparticle aerosols to the efficiency of aerosol filtering methods.

Acknowledgements

Financial support through research project MAT2008-01319/NAN of the Spanish Ministry of Economy and Competitiveness, and EU FP7 NanoValid project #263147 is gratefully acknowledged. F.B. also acknowledges support from the Ramón y Cajal program.

References

Bau S, Witschger O, Gensdarmes F, Thomas D, Borra J-P (2010). Electrical properties of airborne nanoparticles produced by a commercial spark-discharge generator. J Nanopart Res 12:1989–1995.

Biskos G, Vons V, Yurteri CU, Schimidt-Ott A (2008). Generation and sizing of particles for aerosol-based nanotechnology. KONA Powder Part J 26:13-35.

Chen BT, Afshari A, Stone S, Jackson M, Schwegler-Berry D, Frazer DG, Castranova V, Thomas TA (2010). Nanoparticles-containing spray can aerosol: characterization, exposure assessment, and generator design. Inhal Toxicol 22:1072-1082.

Cho K, Chung KS, Biswas P (2011). Coagulation coefficient of agglomerates with different fractal dimensions. Aerosol Sci Technol 45:740-743.

Denny F, Permana E, Scott J, Wang J, Pui DYH, Amal R (2010). Integrated photocatalytic filtration array for indoor air quality control. Environ Sci Technol 44:5558-5563.

Eggersdorfer ML, Pratsinis SE (2012). The structure of agglomerates consisting of polydisperse particles. Aerosol Sci Technol 46:347-353.

Kreyling WG, Biswas P, Messing ME, Gibson N, Geiser M, Wenk A, Sahu M, Deppert K, Cydzik I, Wigge C, Schmid O, Semmler-Behnke M (2011). Generation and characterization of stable, highly concentrated titanium dioxide nanoparticle aerosols for rodent inhalation studies. J Nanopart Res 13:511–524.

Kruis FE, Fissan H, Peled A (1998). Synthesis of nanoparticles in the gas phase for electronic, optical and magnetic applications: A review. J Aerosol Sci 29:511-535.

Geldart D (1973). Types of gas fluidization, Powder Technol 7:285–292.

Grassian VH, Adamcakova-Dodd A. Pettibone JM, O'Shaughnessy PT, Thorne PS (2007). Inflammatory response of mice to manufactured titanium dioxide nanoparticles: Comparison of size effects through different exposure routes. Nanotoxicology 1:211–226.

Guichard JC (1976). Aerosol Generation Using Fluidized Beds, in: Liu BYH (Ed.), Fine Particles: Aerosol Generation, Measurement, Sampling, and Analysis, Academic Press, New York.

Gutierrez L, Gomez L, Irusta S, Arruebo M, Santamaria J (2011). Comparative study of the synthesis of silica nanoparticles in micromixer-microreactor and batch reactor systems. Chem Eng J 171:674-683.

Hinds WC (1999). Aerosol Technology, Wiley, New York.

Jennerjohn N, Eiguren-Fernandez A, Prikhodko S, Fung DC, Hirakawa KS, Zavala-Mendez JD, Hinds W, Kennedy NJ (2010). Design, demonstration and performance of a versatile electrospray aerosol generator for nanomaterial research and applications. Nanotechnology 21:255603.

Jensen KA, Koponen IK, Clausen PA, Schneider T (2009). Dustiness behavior of loose and compacted Bentonite and organoclay powders: What is the difference in exposure risk? J Nanopart Res 11:133-146.

John W (1993). The characteristics of environmental and laboratory-generated aerosols, in: Willeke K, Baron PA (Eds.), Aerosol measurement: Principles, Techniques, and Applications, Van Nostrand Reinhold, New York.

Lind T, Danner S, Guentay S (2010). Monodisperse fine aerosol generation using fluidized bed. Powder Technol 199:232-237

Liu BYH, Lee KW (1975). An aerosol generator of high stability. Am Ind Hyg Assoc J 36:861-865

Liu W, Mazumdar S, Zhang Z, Poussou SB, Liu J, Lin CH, Chen Q (2012). State-of-the-art methods for studying air distributions in commercial airliner cabins. Build Environ 47:5-12.

Lushnikov AA (2010). Introduction to Aerosols. In: Agramovski I, ed. Aerosols - Science and technology. Weinheim: Wiley-VCH, 1-37.

MacMillan AC, Morrison JB, Harmon CW, Nizkorodov SA (2012). Enhancement of surfactants in nanoparticles produced by an electrospray aerosol generator. Aerosol Sci Technol 46:1239-1245.

Myojo T, Oyabu T, Nishi K, Kadoya C, Tanaka I, Ono-Ogasawara M, Sakae H, Shirai T (2009). Aerosol generation and measurement of multi-wall carbon nanotubes. J Nanopart Res 11:91-99.

Pratsinis SE, Kodas TT, Dudukovic MP, Friedlander SK (1986). Aerosol reactor design: Effect of reactor type and process parameters on product aerosol characteristics. Ind Eng Chem Process Des Dev 25:634-642

Pratsinis SE (1988). Simultaneous nucleation, condensation and coagulation in aerosol reactors. J Coll Int Sci 124:416-427.

Prenni AJ, Siefert RL, Onasch TB, Tolbert MA, DeMott PJ (2000). Design and characterization of a fluidized bed aerosol generator: a source for dry, submicrometer aerosol. Aerosol Sci Technol 32:465-481.

Rosati JA, Leith D, Kim CS (2003). Monodisperse and polydisperse aerosol deposition in a packed bed. Aerosol Sci Technol 37:528–535.

Savolainen K, Alenius H, Norppa H, Pylkkänen L, Tuomi T, Kasper G (2010). Risk assessment of engineered nanomaterials and nanotechnologies - A review. Toxicology 269:92-104.

Schmoll LH, Elzey S, Grassian VH, O'Shaughnessy PT (2009). Nanoparticle aerosol generation methods from bulk powders for inhalation exposure studies. Nanotoxicology 3:265-275.

Tsai C, Lin G, Liu C, He C, Chen C (2012). Characteristics of nanoparticles generated from different nano-powders buy using different dispersion methods. J Nanopart Res 14:777.

Van Ommen JR, Valverde, JM Pfeffer R (2012). Fluidization of Nanoparticles: A review. J Nanopart Res 14:737-766.

Vincent JH (2007). Aerosol sampling: science, standards, instrumentation and applications. Chichester: Wiley

Wang Z, Kwauk M, Li H (1998). Fluidization of fine particles. Chem Eng Sci 53:377–395.

Wang CS (2005). Inhaled Particles. Amsterdam: Elsevier.

Wang J, Liu J, Zhang G, Zhou J, Cen K (2011). Orthogonal design process optimization and single factor analysis for bimodal acoustic agglomeration. Powder Technol 210:315–322.

Yao W, Guangsheng G, Fei W, Jun W (2002). Fluidization and agglomerate structure of SiO_2 nanoparticles. Powder Technol 124:152–159.

FIGURE CAPTIONS

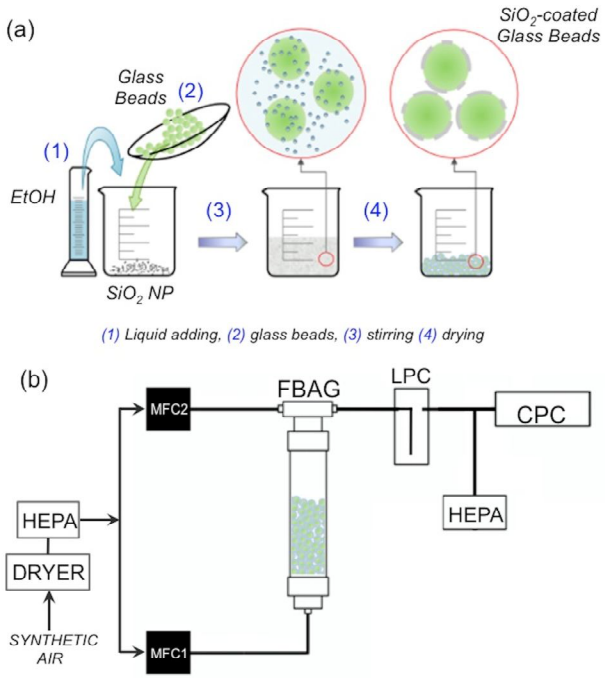

Figure 1. (a) Scheme of the preparation procedure of the silica-coated glass beads for the bed; (b) Diagram of the Fluidized Bed Aerosol Generator (FBAG). (Color figure available online.)

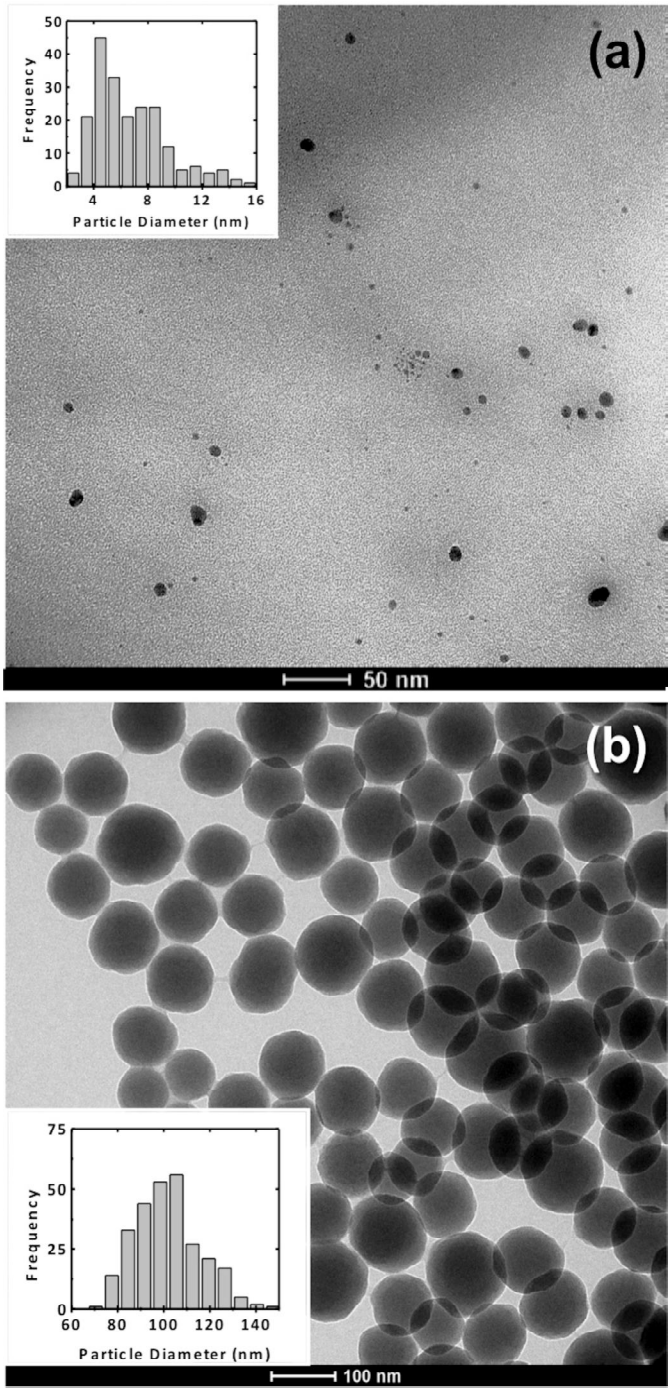

Figure 2. TEM image of the (a) 5-15 nm silica and (b) 100-nm Stöber primary nanoparticles used for coating the glass beads. Insets show histograms of particle size distributions (N = 200) . (Color figure available online.)

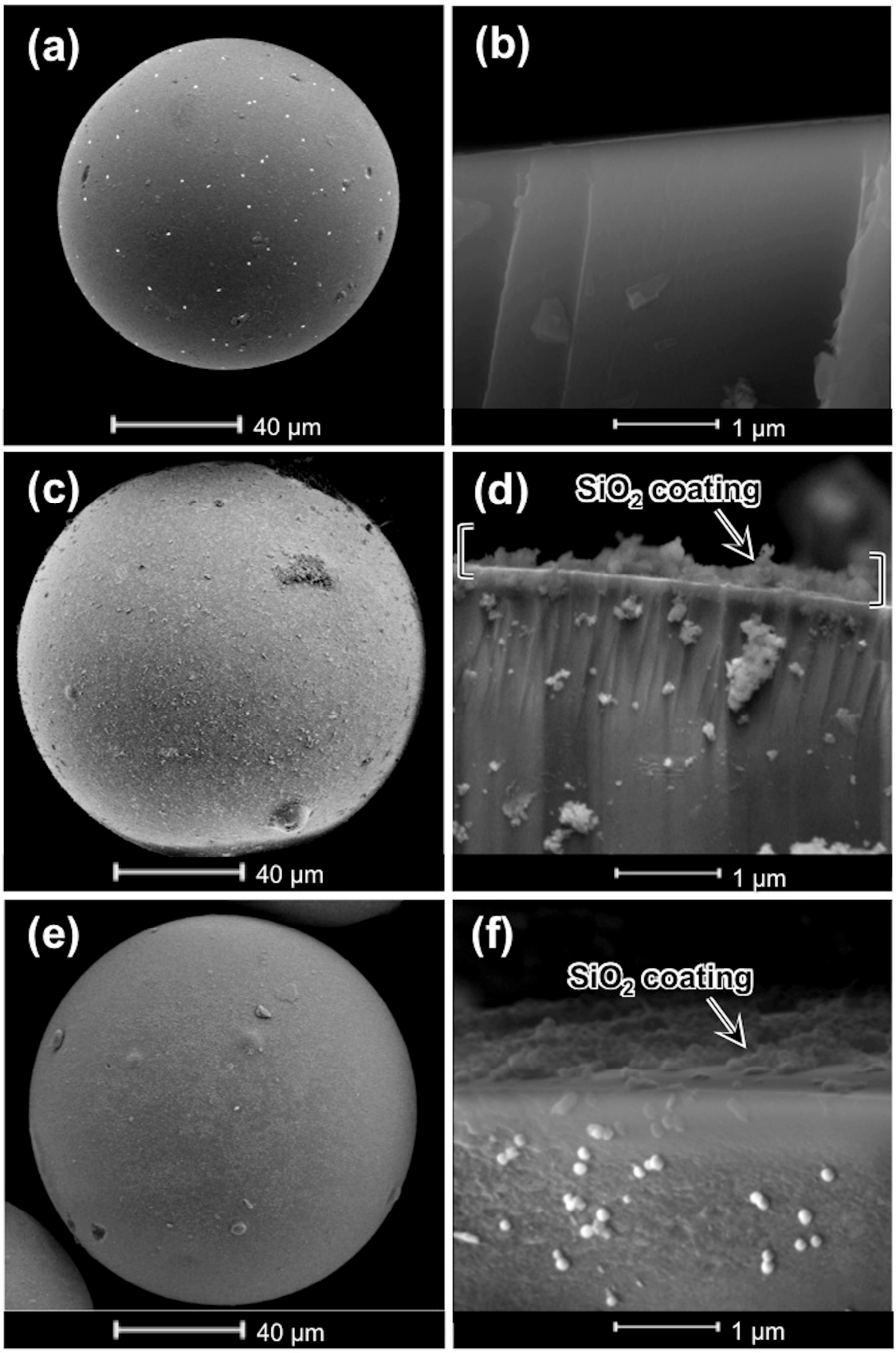

Figure 3. SEM image of the glass beads used for the FBAG: Uncoated glass beads (a, b), 5-15 nm silica-coated glass beads (c, d), 100-nm Stöber silica-coated glass beads (e, f). The cross-sectional close-ups in images (b), (d) and (f) show the changes in surface texture after the coating. (Color figure available online.)

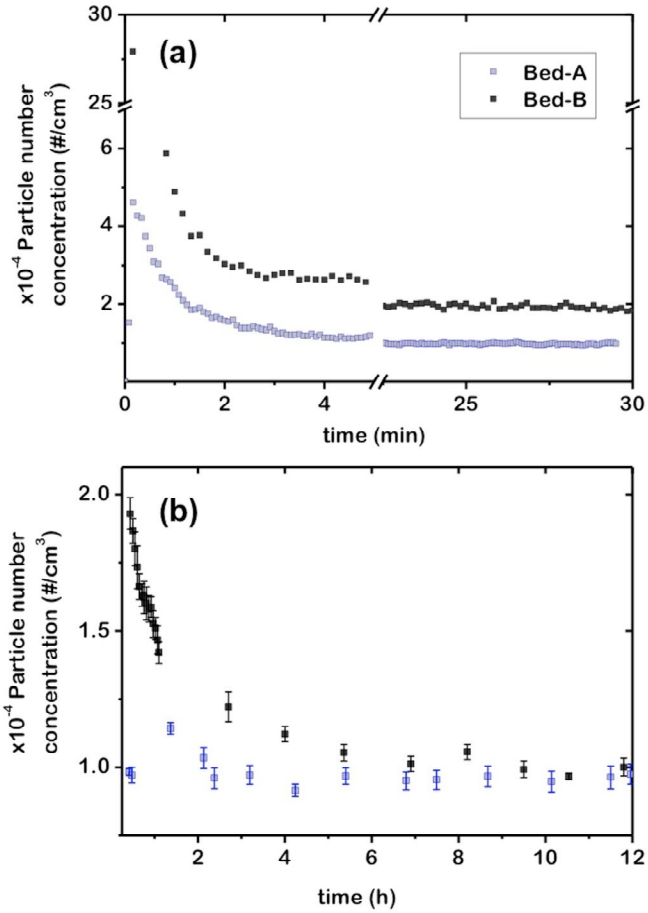

Figure 4. Reproducibility of nanoparticle aerosol generation: number concentration of particles (5 to 1000 nm) for two independent beds (A and B) prepared using the same procedure with 5-15

nm silica-coated glass beads (Q_{FEED} = 1.5 L/min; $Q_{DILUTION}$ = 0.5 L/min and H_B = 5 cm). (Color figure available online.)

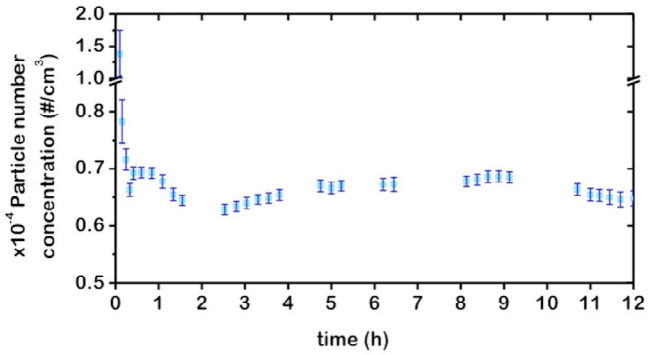

Figure 5. Stability of nanoparticle aerosol generation using glass beads coated with Stöber silica (Q_{FEED} = 1.5 L/min; $Q_{DILUTION}$ = 0.5 L/min and H_B = 5 cm). (Color figure available online.)

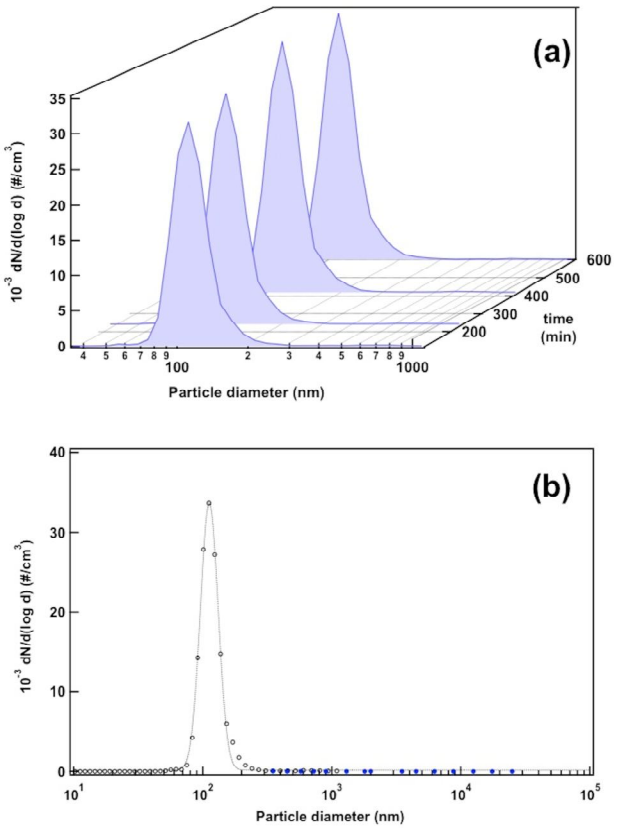

Figure 6. (a) Evolution of particle size distributions using 5-15 nm silica-coated glass beads (conditions of Figure 4) obtained after periodic SMPS+C scans at the FBAG outlet. (b) Average particle size distribution obtained from SMPS+C (open black dots) and OPC data (close blue dots). The data shown correspond to the average of the scans represented in Figure 6a. (Color figure available online.)

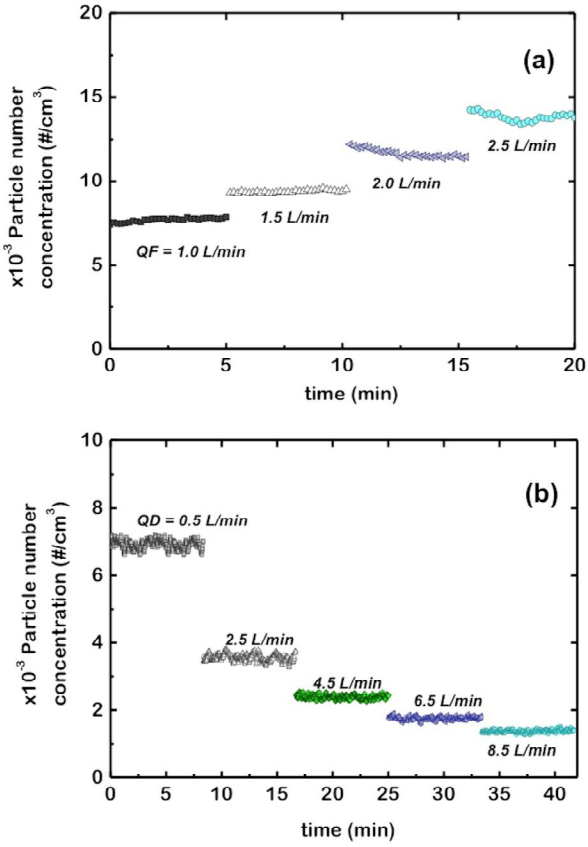

Figure 7. (a) Evolution of particle size distributions using Stöber silica-coated glass beads (conditions of Figure 5) obtained after periodic SMPS+C scans at the FBAG outlet. (b) Average particle size distribution obtained from SMPS+C (open black dots) and OPC data (close blue dots). The data shown correspond to the average of the scans represented in Figure 7a. (Color figure available online.)

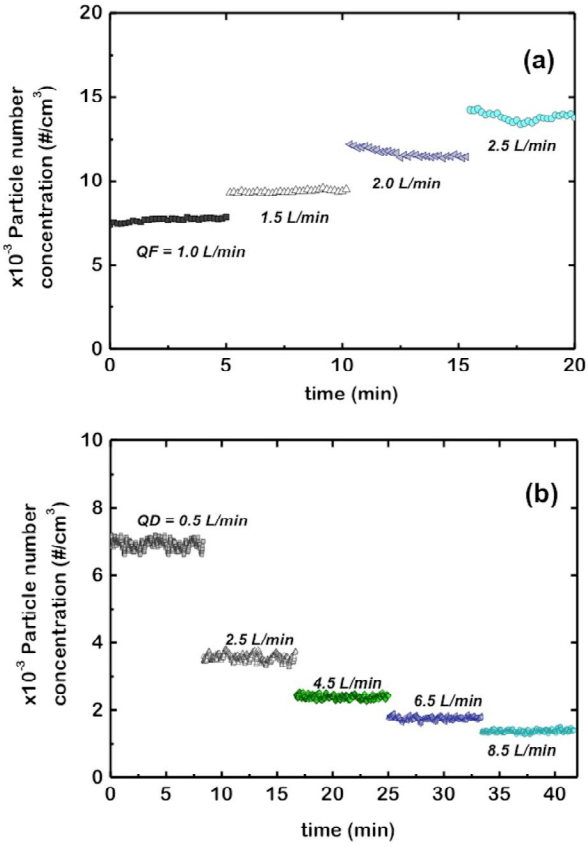

Figure 8. Evolution of the aerosol number concentration of particles (5 to 1000 nm) using 15-nm silica-coated glass beads when the fluidization flow rate (Q_F) was increased step-wise (a) and the dilution flow rate (Q_D) was increased step-wise (b). (Color figure available online.)

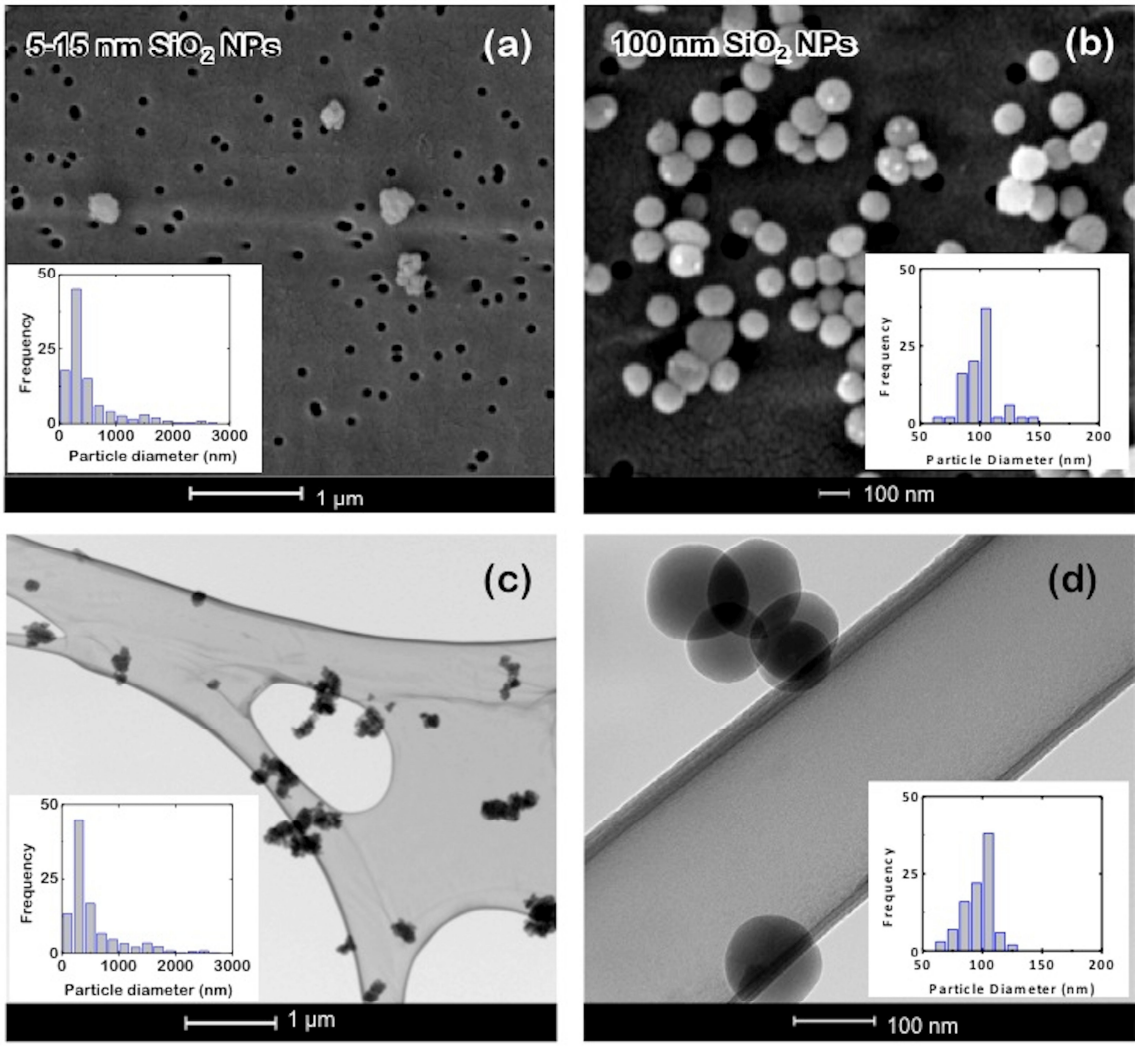

Figure 9. SEM images of filter-collected nanoparticles and size distributions for (a) 5-15 nm silica (N = 448; mean = 336 nm; σ = 2.05) and (b) Stöber nanoparticles (N = 99; mean = 101.1 nm; σ = 14.1 nm); TEM images and size distribution of the holey grid-collected (c) silica nanoparticles (N = 345; mean = 361 nm; σ = 2.01 nm) and (d) Stöber nanoparticles (N = 104; mean = 99 nm; σ = 10.0 nm). (Color figure available online.)